GEONICS LIMITED
1745 Meyerside Dr. Unit 8 Mississauga, Ontario Canada L5T 1C6

Tel: (905) 670-9580
Fax: (905) 670-9204
E-mail: geonics@geonics.com
URL:http//www.geonics.com

TECHNICAL NOTE - TN 17

THE GALVANIC CURRENT COMPONENT IN ELECTROMAGNETIC SURVEYS

J.D. McNeill

March 1985

TABLE OF CONTENTS

INTRODUCTION

In the recent past there has been an increased appreciation of the role played by galvanic currents (also known as current gathering) in the response of the earth as measured with electromagnetic geophysical surveys. It is the purpose of this Technical Note to give a brief introduction, using simple models, to some of the factors that control galvanic current flow.

Consider the generalized prospecting system illustrated in Figure 1; the system operates in either the frequency or time-domain, and target response is measured with a receiver coil which senses the time rate of change of the magnetic field arising from all subsurface current flow.

Associated with the transmitter loop are a primary magnetic field H_e^p and a primary electric field E_e^p. It is convenient to consider the time varying primary magnetic field as inducing vortex currents in the conductive target. If, furthermore, the ground has finite conductivity, the primary electric field will cause currents to flow, which, in the vicinity of the more conductive target, will become concentrated. We shall call these currents the galvanic currents, to distinguish them from the vortex currents within the target, but we must emphasize that in fact all current flow is caused by the electric field generated by the time varying primary magnetic field.

Now in general the measured magnetic field (or its time-derivative) will reflect both a vortex and galvanic current contribution. At very early times in a time-domain system, or at very high frequencies in a frequency-domain system,

the total response to the primary electromagnetic field will be complex, due in part to interaction effects between the vortex and galvanic currents. At more moderate times, or frequencies, the interaction may become relatively insignificant and it should then be possible to view the vortex and galvanic currents as existing independently. For most of this Technical Note we will assume that this is the case. Our interest will lie principally in the primary electric field and resultant galvanic current flow; the generation of vortex or eddy currents in a conductive target is relatively well understood and will be mentioned only briefly.

It has been suggested in a recent paper by McNeill et al (1984) that, with large loop transient systems, the electric field response can at certain measurement times totally dominate the overall response. It is becoming apparent that this fact is also correct for other system configurations. In particular it should be noted that although we have shown a transmitter loop in Figure 1, both VLF and magneto-telluric sources generate the electric and magnetic field components shown in the figure. Whether or not the electric field response dominates for any specific survey configuration is a function of, amongst other variables, the ratio of the primary electric to magnetic field strength at the target. This ratio is a function of transmitter type and frequency; whenever the ratio is high, as for large loop transmitters or plane wave sources, it is quite possible that the electric field response will dominate.

PARALLEL PLATE CAPACITOR MODEL

Although we will eventually discuss a prolate spheroid model, which is a reasonable approximation to certain types of ore bodies, it will be useful to start with a simpler model so as to review some basic physics.

Figure 2 shows a parallel plate capacitor connected to a DC source of voltage. It will be assumed that the length and height of the end plates is much greater than the separation between them so that fringing can be ignored and the geometry can be treated as one-dimensional.

Assume initially that the material within the capacitor has a conductivity σ_e.

If A is the area of the end plates and d the distance between them, the current that flows is given by

$$I = V\sigma_e \frac{A}{d}$$

and the current density J_e everywhere within the material is given by

$$J_e = \frac{I}{A} = \sigma_e \frac{V}{d}$$

or $$J_e = \sigma_e E_e$$

where E_e (equal to V/d) is the electric field.

Suppose that we now allow a thin layer of material in the center of the capacitor to have a conductivity $\sigma_i > \sigma_e$. If this layer is very thin compared with d, its resistance will be negligible compared with that of the material on either side, the current will still be I and the current density in the surrounding material still $J_e = \sigma_e E_e$. From the law of continuity of current we know that J_i, the current density within the thin layer, must be equal to J_e. Therefore $J_e = \sigma_e E_e = J_i = \sigma_i E_i$, where E_i is the electric field in the thin layer. But since $\sigma_i > \sigma_e$ it is clear that E_i is less than E_e; within the layer a secondary electric field E_s, in opposition to E_e, must have been generated so as to reduce the total field, i.e. $E_i = E_e + E_s$, where E_s is oppositely directed to E_e and thus negative. But the source of static electric fields is electric charges, and it is charges, uniformly induced over the entire surface at each interface, which generate E_s as shown in detail in Figure 3 (that E_s results from the induced surface charges is emphasized by the dashed portion in the figure).

It is of interest to calculate the magnitude of these induced charges as a function of σ_i. This is easily done since we know that $J_i = J_e$ and therefore

$$\sigma_e E_e = \sigma_i E_i = \sigma_i (E_e + E_s)$$

$$E_s = E_e \frac{(\sigma_e - \sigma_i)}{\sigma_i}$$

$$= E_e \frac{\left[1 - \frac{\sigma_i}{\sigma_e}\right]}{\frac{\sigma_i}{\sigma_e}}$$

If S is the induced surface charge density on the right hand interface we can apply Gauss' Law to a small cylinder located at this interface to obtain

$$S = \varepsilon_o(E_e - E_i)$$

whereupon

$$\frac{S}{\varepsilon_o E_e} = \frac{\left[1 - \frac{\sigma_i}{\sigma_e}\right]}{\frac{\sigma_i}{\sigma_e}}$$

where $\varepsilon_o = 10^{-9}/36\pi$ (permittivity of free space).

This quantity is plotted in Figure 4, along with $E_i/E_e = 1/(\sigma_i/\sigma_e)$.

It is instructive to work out a few values for the various quantities.

Let E_e=1V/m, σ_e=1 mho/m and let the arrows indicate the field directions

σ_i (mho/m)	E_e (v/m)	S/ε_o (v/m)	E_s (v/m)	E_i (v/m)	$J_i=\sigma_i E_i$ (amp/m²)
1	1→	0	0	1→	1
2	1→	$\frac{1}{2}$	← $\frac{1}{2}$	$\frac{1}{2}$→	1
4	1→	$\frac{3}{4}$	← $\frac{3}{4}$	$\frac{1}{4}$→	1
10	1→	$\frac{9}{10}$	← $\frac{9}{10}$	$\frac{1}{10}$→	1

As the center layer is made more conductive the induced surface charge density at the interfaces increases. This increases the secondary field E_s (which opposes the primary field E_e) and thus reduces the total internal electric field E_i by exactly the right amount to account for the increased

conductivity, maintain the current density unchanged and therefore continuous across the interface. This is evident from Figure 4 where we see that as σ_i/σ_e increases, the total internal electric field E_i decreases as $(\sigma_i/\sigma_e)^{-1}$ so that the internal current density (given by $\sigma_i E_i$) remains constant.

We now understand that it is the induced charge density that controls the secondary field, the total internal electric field, and thus the internal current density given by $J_i = \sigma_i E_i$.

CONDUCTIVE CIRCULAR CYLINDER

For our next simple model we will take a two-dimensional conductive circular cylinder in a uniform static electric field perpendicular to the axis as shown in Figure 5A. Although the cylinder is a 2D model the results will be very much like those for a sphere; we use the cylinder because the surface charge density calculations are conveniently available from Kaufman and Keller (1981), as are the results for our next and more interesting model, an elliptical cylinder. The results from the elliptical cylinder will be used to understand the response of the prolate spheroid.

In our previous example the external electric field was everywhere perpendicular to the interface, which is not the case for the cylinder. However it is the component of E_e normal to the surface of the cylinder (or normal to the interface between any two media of different conductivities) which causes surface charges to be induced at the interface. It is well known that, for the cylinder, these charges are distributed in such a fashion on the surface as to produce

a uniform secondary electric field E_s in the interior which is again in opposition to the primary field, thus reducing the total internal electric field E_i. Externally these induced charges produce a secondary electric field which also opposes the primary electric field, as indicated in Figure 5A. The net result is that the lines of current density (given externally by $J_e=\sigma_e E_e$ and internally by $J_i=\sigma_i E_i$) are as shown in Figure 5B. In the interior of the cylinder the total electric field has been reduced by the induced surface charges; however unlike the parallel plate capacitor the reduction has not been quite enough to compensate for the increased conductivity of the cylinder, with the result that the current density is greater inside the cylinder than outside. This is evident in Figure 4, where we see that at low values of conductivity contrast the induced charge density on the surface of the cylinder does not increase quite as quickly as for the parallel plate capacitor, with the result that the opposing secondary electric field E_s does not become quite large enough to cause the total internal electrical field E_i to be reduced by the right amount to compensate for the increased conductivity. Thus, unlike the parallel plate capacitor, as σ_i increases the internal current density J_i also increases. Eventually however, as we continue to increase σ_i, the induced charge density does become large enough to correctly compensate for the increase in σ_i; further increases in σ_i do not produce an increase in J_i, which has become saturated.

It is illustrated by Kaufman and Keller (1981) that for the cylinder the normalized induced charge density and thus the secondary electric field E_s varies with conductivity contrast as

$$\frac{E_s}{E_e^p} = \frac{\left[1- \frac{\sigma_i}{\sigma_e}\right]}{\left[1+ \frac{\sigma_i}{\sigma_e}\right]}$$

and the total internal electric field E_i as

$$\frac{E_i}{E_e^p} = 1 + \frac{\left[1 - \frac{\sigma_i}{\sigma_e}\right]}{\left[1 + \frac{\sigma_i}{\sigma_e}\right]} = \frac{2}{\left[1 + \frac{\sigma_i}{\sigma_e}\right]}$$

and the current density J_i (normalized with respect to $J_e = \sigma_e E_e^p$) as

$$\frac{J_i}{J_e} = \frac{2 \quad \frac{\sigma_i}{\sigma_e}}{\left[1 + \frac{\sigma_i}{\sigma_e}\right]}$$

This quantity is illustrated in Figure 6 where it is observed that significant variation of J_i/J_e takes place over rather limited range of σ_i/σ_e, becoming saturated at 2.0 as σ_i/σ_e increases above 10. Thus measurement of any quantity related to J_i (such as magnetic field components) will give very little information about target conductivity.

Figure 7A illustrates the distribution of surface charge density on the surface of the cylinder for various values of σ_i/σ_e. The density increases essentially linearly with distance from the center for all values of σ_i/σ_e.

CONDUCTIVE ELLIPTICAL CYLINDER

Let us now consider the conductive elliptical cylinder shown in Figure 8. Once again the component of E_e normal to the surface causes surface charges to be induced at the interface, again producing a uniform internal secondary field E_s in opposition to the primary field E_e^p. However when a/b is much

greater than unity there is an important difference between this target and the circular cylinder; now the location of the major induced charge density lies essentially at the ends of the target, and the secondary electric field everywhere in the interior of the conductor is smaller than for the circular cylinder, even though the induced charge density is larger.

The result is that for $a/b \gg 1$ the secondary electric field E_s is essentially zero within the target, $E_i \cong E_e$, and the current J_i, being given by $\sigma_i E_i \cong \sigma_i E_e$, can rise to large levels if $\sigma_i/\sigma_e \gg 1$. Since the charges are remotely located, the response does not saturate until large values of σ_i/σ_e are reached. This is shown by the equations for the secondary electric field

$$\frac{E_s}{E_e^p} = \frac{\left[1 - \frac{\sigma_i}{\sigma_e}\right]}{\left[\frac{a}{b} + \frac{\sigma_i}{\sigma_e}\right]}$$

and the total internal electric field

$$\frac{E_i}{E_e^p} = \frac{\left[\frac{a}{b} + 1\right]}{\left[\frac{a}{b} + \frac{\sigma_i}{\sigma_e}\right]}$$

and the enhanced current density

$$\frac{J_i}{J_e} = \frac{\frac{\sigma_i}{\sigma_e}\left[\frac{a}{b} + 1\right]}{\left[\frac{a}{b} + \frac{\sigma_i}{\sigma_e}\right]}$$

Thus for the extended target ($a/b \gg 1$) the response varies more slowly with σ_i/σ_e and measurement of the magnetic field (or its time derivative) is now more diagnostic of the target conductivity. Furthermore for extended targets of high conductivity contrast ($\sigma_i/\sigma_e \gg a/b$)

$$\frac{J_i}{J_e} \cong \left[\frac{a}{b} + 1\right]$$

and this relatively large current flow (compared with 2 for the circular cylinder) will produce a more detectable anomaly.

PROLATE SPHEROID - Current Flow

But none of these targets are useful for modeling conductive ore bodies, which are often blobby, or plate-like. For the former targets a prolate spheroid is appropriate, and its response will also give a good indication of the response for a plate.

Kaufman and Keller (1981) give a detailed treatment of the response of a three dimensional prolate spheroid located in an axial electric field as shown in Figure 9. The results are quite similar to those for the elliptical cylinder discussed above. They show that the total internal electric field is given by

$$\frac{E_i}{E_e^p} = \frac{1}{1+[(\sigma_i/\sigma_e)-1]L}$$

and thus the enhanced current density by

$$\frac{J_i}{J_e} = \frac{\sigma_i/\sigma_e}{1+[(\sigma_i/\sigma_e)-1]L}$$

where L, the depolarization factor, is given by

$$L = \frac{1-e^2}{2e^3}\left[\log_e \frac{1+e}{1-e} - 2e\right]$$

where $e = [1-(b^2/a^2)]^{\frac{1}{2}}$

Now if a>>b $L \cong (\frac{b}{a})^2[\log_e(\frac{2a}{b}) - 1]$

$$L \cong K(\frac{b}{a})^2$$

where K is a slowly varying function of b/a, of the order of 3 for typical targets. In this case

$$\frac{J_i}{J_e} \cong \frac{(\frac{a}{b})^2 \frac{\sigma_i}{\sigma_e}}{\left[(\frac{a}{b})^2 + K\frac{\sigma_i}{\sigma_e}\right]}$$

Once again J_i/J_e increases linearly with σ_i/σ_e until large values of σ_i/σ_e are reached, as shown in Figure 10A. Again measurement of B or $\dot{B}$ will be diagnostic of target conductivity over a wide range for elongated targets. The overall current flow in the vicinity of a relatively conductive spheroid is shown schematically in Figure 11A. It is clear that the concentration of current in an extended spheroid can produce a very detectable target having the spatial characteristics of a line source for measurements made near the center of the target.

If the spheroid is less conductive than the surrounding medium, Figure 10A shows that for $\sigma_i/\sigma_e < 1$, J_i/J_e is also less than unity. For the sphere (a/b=1) the induced charges, now of opposite sign than for the more conductive target, generate a secondary electric field in the same direction as E_e, slightly increasing E_i, with the result that J_i/J_e does not fall as quickly as σ_i/σ_e. For more elongated resistive targets the charges produce a smaller electric field inside the body, $E_i \cong E_e$, and J_i/J_e decreases directly with σ_i/σ_e. Figure 11B illustrates schematically the current flow for an infinitely resistive spheroid.

Figure 10B is a replot of Figure 10A with σ_i/σ_e fixed and a/b allowed to vary. We see that, for large a/b, J_i/J_e approaches σ_i/σ_e asymptotically as shown by the equation, but that for large σ_i/σ_e, large values of a/b [$\cong 10(\sigma_i/\sigma_e)^{\frac{1}{2}}$] are required. For example suppose that b=1 m, and σ_i/σ_e=100. Instinctively one would expect that for a=10 m the target would be long enough for end effects to be negligible. Figure 10B demonstrates that this is definitely not the case. The graph illustrates that the galvanic response from elongated, three dimensional high conductivity contrast targets can still be significantly less than the response from two dimensional targets. Caution must be exercised when applying the results of two dimensional modeling to the interpretation of three dimensional responses.

PROLATE SPHEROID - Approximate Plane Wave Target Response

We would like to obtain a rough estimate of the plane wave response from the galvanic component for the two and three dimensional bodies described in the

previous section. Kaufman and Keller (1981) present equations for the azimuthal magnetic field component H_ϕ, measured in the equatorial plane at a distance r from the center of a prolate spheroid subjected to a uniform axial electric field and located in a homogeneous whole space (Figure 12). For plane wave excitation the primary electric field is simply related to the primary magnetic field by the intrinsic impedance of the ground so that the ratio H_ϕ/H_e^p is easily calculated. In Figure 13 we show the results of calculations of the anomalous horizontal magnetic field divided by the primary magnetic field for a very slim spheroid of radius b=3 m buried at a depth r of 20 m. The calculations are indicative of the response to plane wave excitation at VLF frequencies (20kHz) and the ground conductivity has been assumed to be 0.001 mho/m so that skin depth attenuation is negligible; the target half-length (a) and conductivity (σ_i) are varied. The general shape of the curves is similar to those of Figure 10B, modified at low values of a/b by the fact that the target length is becoming comparable to the depth of burial so that the target no longer responds geometrically as a linear source.

For greatly extended conductive targets such that, $a/b >> (\sigma_i/\sigma_e)^{\frac{1}{2}}$, $E_i \cong E_e^p$, $J_i \cong \sigma_i E_e^p$ and we would expect that the response should be approximately the same as that from a line source carrying a current $I = \pi b^2 J_i$. This is easily verified by applying Amperes Law to get the magnetic field from a line source at distance r.

$$2\pi r H_\phi = I$$

$$H_\phi = \frac{b^2 \sigma_i E_e}{2r}$$

For plane wave excitation E_e^p and H_e^p are related by

$$\frac{E_e^p}{H_e^p} = \left[\frac{\omega\mu}{\sigma_e}\right]^{\frac{1}{2}}$$

whence

$$\frac{H_\phi}{H_e^p} = \frac{b^2 \sigma_i}{2r}\left[\frac{\omega\mu}{\sigma_e}\right]^{\frac{1}{2}}$$

where

$$\omega = 2\pi f \quad (f=20\text{kHz})$$

$$\mu = 4\pi \times 10^{-7} \text{ h/m}$$

Using b=3 m, r=20 m, $\sigma_e=10^{-3}$ mho/m we arrive at

σ_1 =	0.01	0.1	1	10 mho/m
$\frac{H_\phi}{H_e^p}$ =	0.0284	0.284	2.84	28.4

in excellent agreement with Figure 13, even for σ_i=0.01 mho/m (a conductivity contrast of only 10).

For VLF surveys the limit of detectability is an anomaly of about 2% of the primary magnetic field strength, a level which is indicated on the figure. This spheroid would be clearly detectable as long as σ_i is greater than about 0.03 mho/m and the half-length a greater than 50 m. Higher conductivity or larger a will make a large anomaly indeed. We can conclude that, at least for

plane wave excitation, relatively poorly conductive targets will be quite detectable as a result of their galvanic current response if they are reasonably long. It will be true that most of the targets observed from VLF surveys will be long ones and they need not be terribly conductive.

The dashed response on Figure 12 is 10 times the response from a relative insulator ($\sigma_i=10^{-4}$ mho/m) which gives an anomaly of opposite sign from a conductor. Although the anomaly from this particular insulator (b/r=3/20) is not detectable the response from large, near-surface insulators certainly will be.

Finally, the measured response will, of course, be further complicated by the presence of vortex or eddy currents in the target, induced by the time-varying primary magnetic field; however it now appears that for plane wave systems operating at VLF frequencies and below, the contribution from vortex currents will be negligible in all but the most resistive ground. In Figure 13 the vortex current response for the two most conductive 2D cylinders is seen to be below the detection limit.

CIRCULAR CYLINDER IN AXIAL ELECTRIC FIELD

To this point we have dealt with static fields, assuming that the results will be appropriate for time-varying fields.

Let us now turn our attention to a conductive infinite circular cylinder located in an axial electric field and a perpendicular magnetic field as shown in Figure 14. We will allow the fields to be time-varying but will

assume that the ground conductivity σ_e is sufficiently low that δ_e (the skin-depth in the ground) is much larger than a, the radius of the cylinder, so that the primary electric and magnetic fields are essentially constant over the cross section of the cylinder, which can thus be considered as being located in uniform primary electric and magnetic fields.

As shown by Kaufman and Keller (1981), under this condition the external secondary fields can be expressed in the form (a time dependence given by $e^{-i\omega t}$ has been assumed)

$$E_x = E_e^p A_o K_o (k_e r) + 2H_e^p Z_e A_1 K_1 (k_e r) \cos\phi$$

$$H_\phi = \frac{E_e^p}{Z_e} A_o K_o' (k_e r) + 2H_e^p A_1 K_1' (k_e r) \cos\phi$$

$$H_r = 2H_e^p A_1 \frac{K_1 (k_e r)}{k_e r} \sin\phi$$

where $Z_e = (-i\omega\mu/\sigma_e)^{\frac{1}{2}}$

In these equations $K_o(k_e r)$ and $K_1(k_e r)$ are modified Bessels functions, $k_e^2 = -i\mu\sigma_e\omega$, $k_i^2 = -i\mu\sigma_i\omega$, and A_o and A_1 are functions of $(k_i a)$ which describe the behaviour of E_x, H_ϕ, and H_r with the induction number $(k_i a)$. The zero-order terms do not show a ϕ dependence and represent the response from an infinitely long line current source. The first-order terms with $\cos\phi$ or $\sin\phi$ dependence represent the response from an infinitely long line of magnetic dipoles. In accord with our earlier comments we will call the zero-order terms the galvanic current component, generated by the primary electric field, and the first-order terms the vortex current component, generated by the time varying primary magnetic field. Thus the secondary electric field from the

galvanic source is given by

$$E_{x_o} = E_e^p A_o K_o (k_e r)$$

and the secondary magnetic field by

$$H_{\phi_o} = \frac{E_e^p}{Z_e} A_o K_o' (k_e r)$$

$$= \frac{E_e^p}{Z_e} A_o K_1 (k_e r)$$

Kaufman and Keller proceed to show further that, if $\delta_i >> a$

$$E_{x_o} \cong i \frac{\omega\mu}{2} a^2 (\sigma_i - \sigma_e) E_e^p K_o (k_e r)$$

$$H_{\phi_o} \cong k_e^2 \frac{a}{2}^2 (\sigma_i - \sigma_e) E_e^p K_1 (k_e r)$$

therefore

$$E_{x_o} \cong \frac{i\omega\mu I}{2\pi} K_o (k_e r)$$

$$H_{\phi_o} \cong \frac{k_e I}{2\pi} K_1 (k_e r)$$

where $$I = \pi a^2 (\sigma_i - \sigma_e') E_e^p$$

Thus the linear source secondary field terms external to the cylinder are indeed those that would be calculated from an axial current filament of strength $a^2(\sigma_i - \sigma_e)E_e^p$, in agreement with our earlier results. Again, in

the two dimensional limit (an infinite cylinder) of the three dimensional spheroid, the regions of high charge density are located at infinity and the internal current J_i continues to increase with σ_i/σ_e without limit, as would be expected from our earlier discussion of the spheroid. Of course J_i does not really increase without limit, but it is no longer the influence of the absent end charges that cause it to be bounded. As σ_i/σ_e gets very large the condition $\delta_i >> a$ is no longer fulfilled and the current becomes concentrated by skin-depth effects in the vicinity of the circumference of the cylinder (as a cylindrical shell) rather than being relatively uniformly distributed throughout the cross-section as required for the current filament approximation discussed above. Once the current is confined to flow near the surface of the cylinder the impedance increases as the effective cross-sectional area is reduced, preventing unlimited current flow with increasing σ_i.

DISCUSSION

It has been assumed throughout most of this Technical Note that a simple analysis of galvanic current flow made on the basis of a static field approximation is still valid over a reasonably wide range of frequencies and times. For the example of the infinitely long circular cylinder this assumption was shown to be correct as long as the radius of the conductive cylinder was much less than a skin-depth in either the external or internal material. For other geometries similar constraints on cross-sectional dimensions in terms of a skin-depth will also apply. In general such simplified analyses will assist in our understanding of the results of more

accurate (and more difficult) calculations as they become available.

The principle result of the analysis has been to show that, at least for plane wave excitation, long, thin relatively poorly conductive targets oriented approximately parallel to the primary electric field will give large magnetic field anomalies as a result of galvanic current flow, when their vortex current component is probably quite insignificant. This is true at VLF frequencies, and will be even truer at lower frequencies (AMT and MT) since, although the ratio of electric to magnetic field in the earth decreases as $\omega^{\frac{1}{2}}$, the secondary fields due to vortex currents decrease more rapidly ($\cong\omega$ for the quadrature phase and ω^2 for the inphase response). For targets less well aligned with the primary electric field the galvanic response will be reduced. So too will the vortex current response, due to reduced coupling with the primary magnetic field.

Thus for plane wave excitation at low frequencies it is anticipated that the majority of anomalies encountered during surveys in all but the most resistive terrain will be caused by galvanic current response from relatively poorly conductive targets. This may also be true for large transmitter loop systems which generate a relatively large electric field, as suggested by McNeill et al (1984). In as much as various electromagnetic methods produce different ratios between primary electric and primary magnetic field strengths the relative contribution from galvanic and vortex currents will also be different.

Contrary to a remark made by McNeill et al (1984) it has been shown in this Technical Note that for reasonably extended targets the galvanic current response fortunately continues to be a function of σ_i/σ_e over a wide range, so that measurements of the magnetic response arising from the galvanic component are often diagnostic of target conductivity.

It has been shown that the galvanic current response from relatively long conductive targets is still significantly less than the response from the equivalent two-dimensional target, if the conductivity contrast is high.

Finally, in discussions concerning the response from two dimensional targets located in conductive ground and excited by time-varying line sources, it sometimes appears to be assumed that there are no vortex currents present. As we have seen in the previous section there is still vortex current flow although it may be relatively small. One also hears that for this geometry there is no current gathering. Whilst it is true that there are no effects from charges at the absent conductor ends there may be an even larger axial current component which gives the same spatial response over the target center as the so-called current gathering.

Perhaps rather than using the term "current gathering" it would be preferable (remembering that currents diverge past relatively resistive objects as well as converge through relatively conductive targets) to use the term "galvanic current" for the current component which causes the zero order term in the response, and "inductive current" for the component which causes the first order term (and in the case of a non-uniform primary

field, the higher order terms). It is reasonable to consider that the galvanic current is proportional to the primary electric field while inductive currents are proportional to the time rate of change of the primary magnetic field, and the arbitrary restriction to two or three dimensional targets is removed.

ACKNOWLEDGEMENTS

The author would, as always, like to express his gratitude to Dr. Alex Kaufman at the Colorado School of Mines for enumerable stimulating and enlightening conversations on our favourite topic.

BIBLIOGRAPHY

Kaufman, A.A., and Keller, G.V., 1981, The magneto-telluric sounding method: Amsterdam, Elsevier Scientific Publishing Co.

McNeill, J.D., Edwards, R.N., and Levy, G.M., 1984, Approximate calculations of the transient electromagnetic response from buried conductors in a conductive half-space. Geophysics, v.49, p.918-924.

Figure 1 Electromagnetic Field Components and Currents

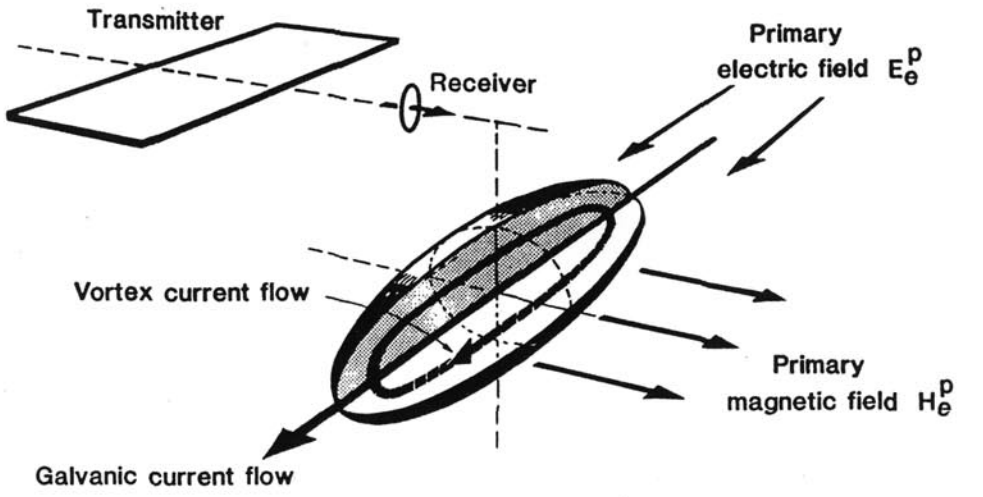

Figure 2 Parallel Plate Capacitor

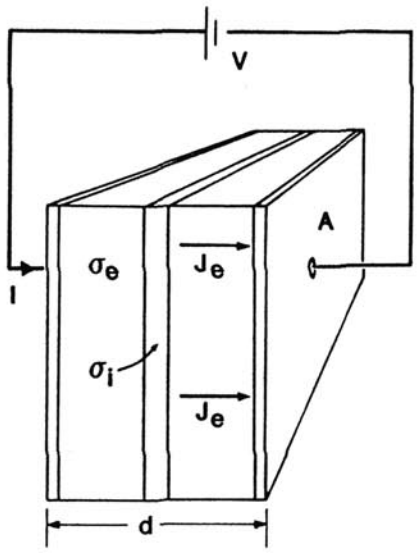

Figure 3 Detail near the Thin Layer

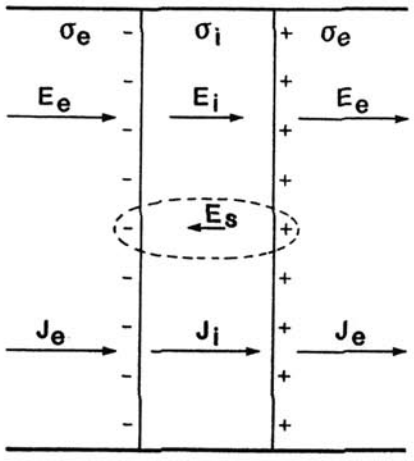

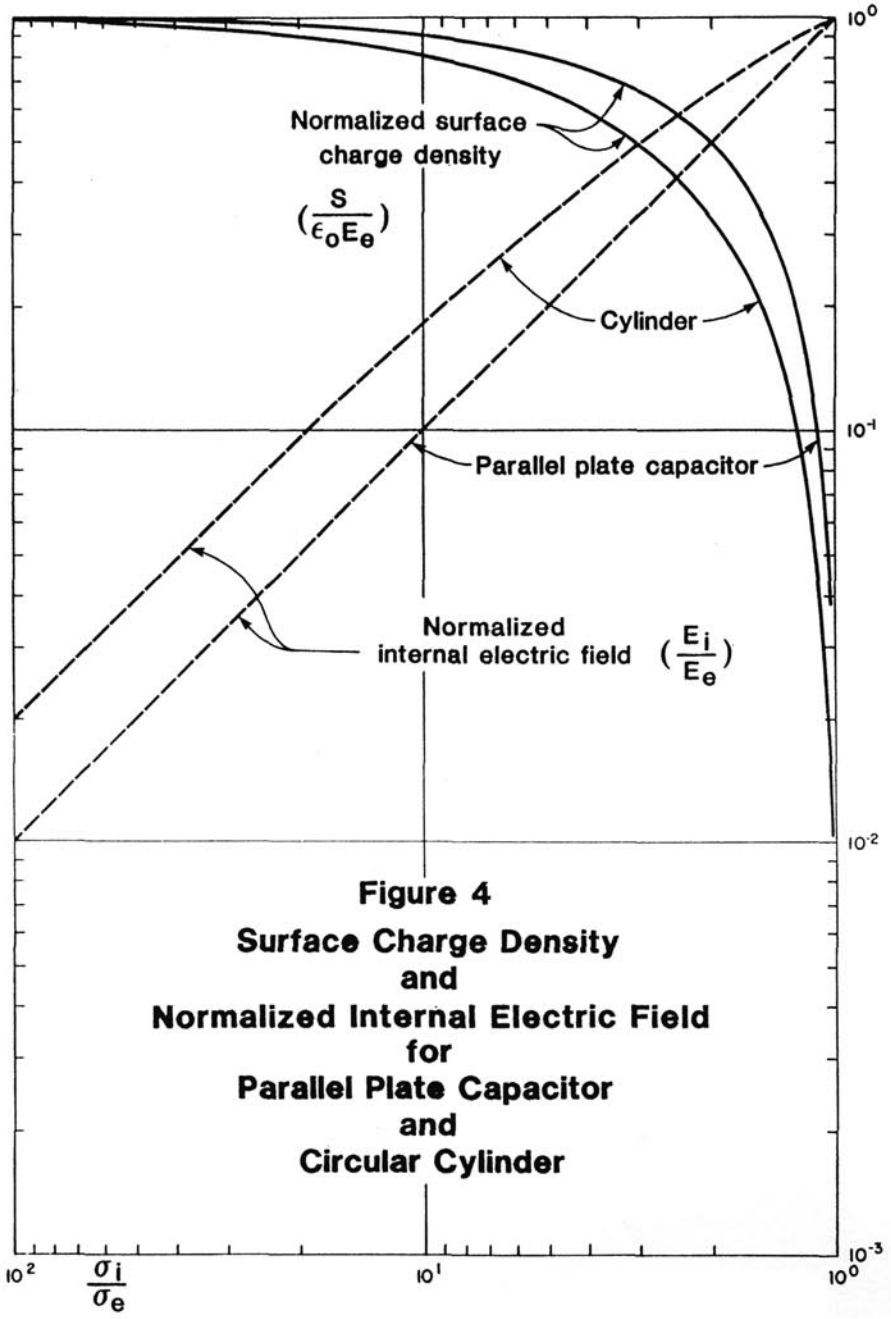

Figure 4
Surface Charge Density
and
Normalized Internal Electric Field
for
Parallel Plate Capacitor
and
Circular Cylinder

Figure 5a Electric Field in vicinity of Conductive Circular Cylinder

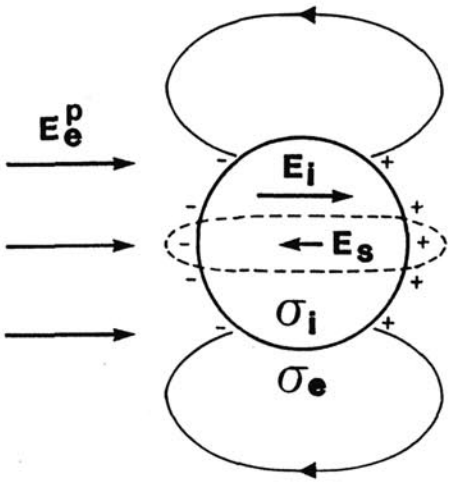

Figure 5b Current Flow in vicinity of Circular Cylinder

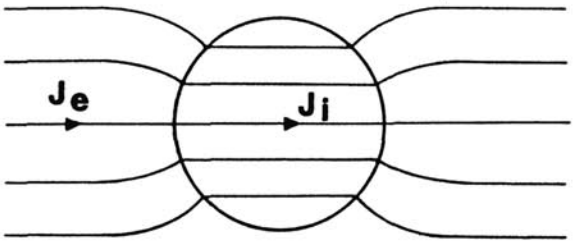

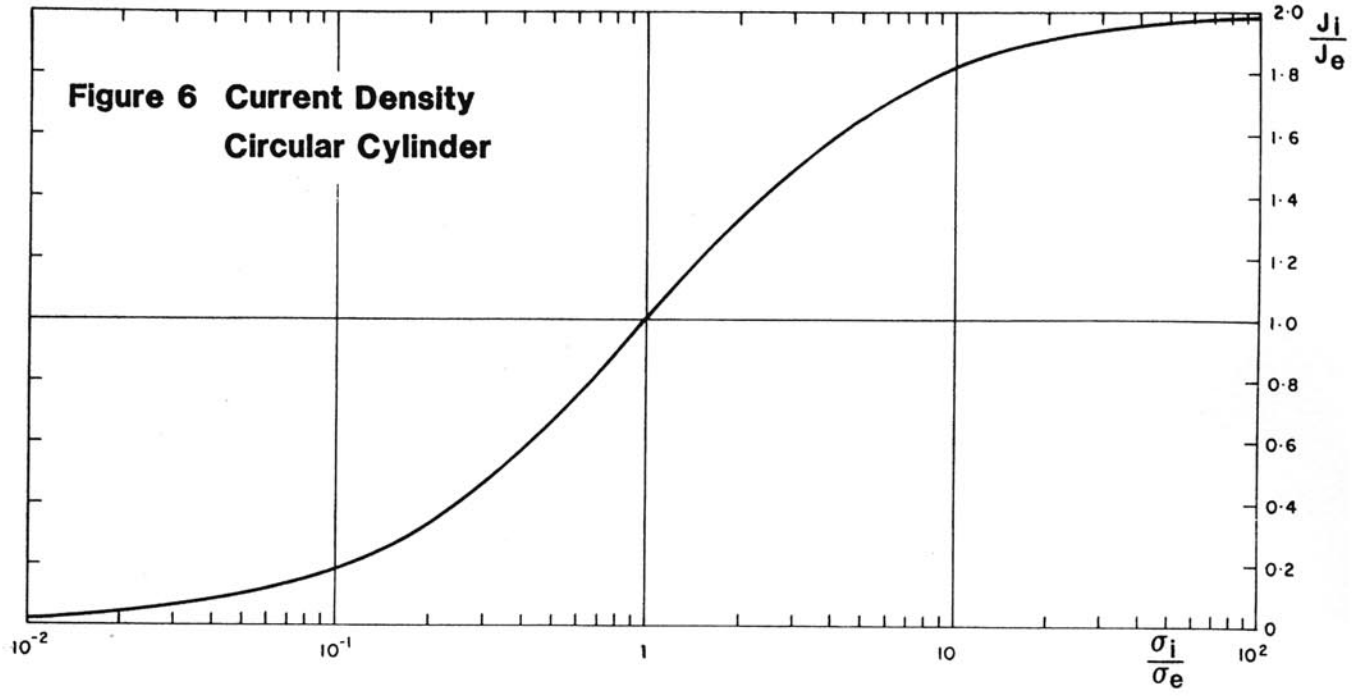
Figure 6 Current Density
Circular Cylinder
2·0
1·8
1·6
1·4
1·2
1·0
0·8
0·6
0·4
0·2
0
$\frac{J_i}{J_e}$
10^{-2}
10^{-1}
1
10
10^2
$\frac{\sigma_i}{\sigma_e}$

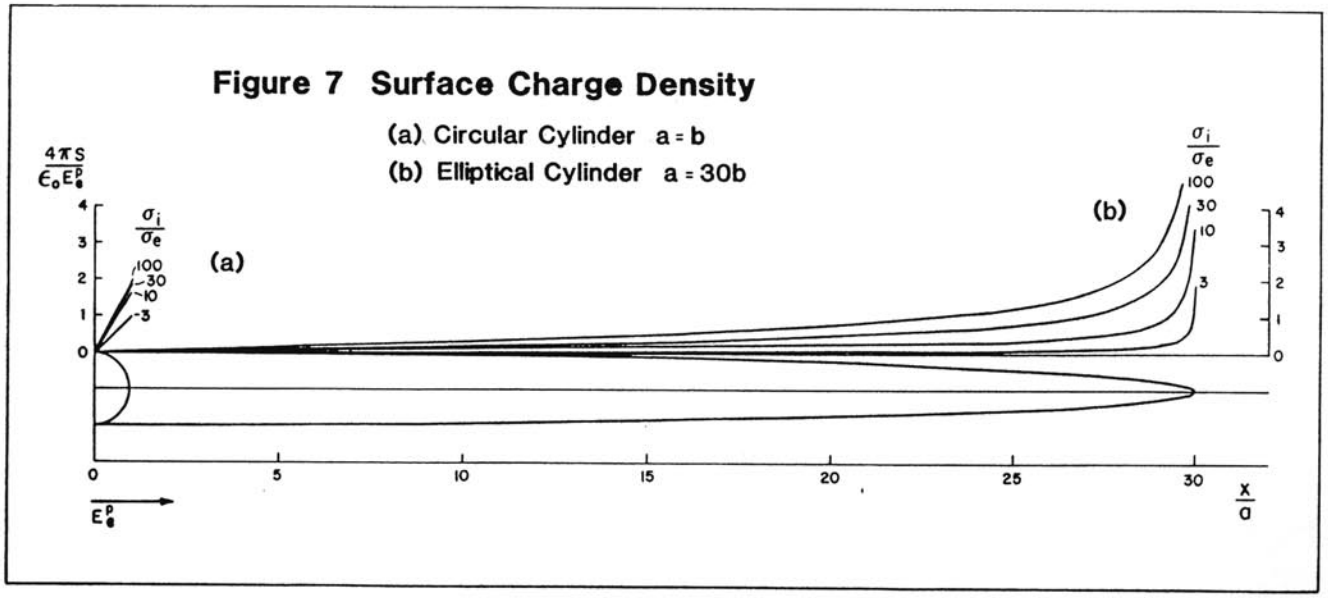
Figure 7 Surface Charge Density
(a) Circular Cylinder a = b
(b) Elliptical Cylinder a = 30b
$\frac{4\pi S}{\epsilon_o E_e^p}$
$\frac{\sigma_i}{\sigma_e}$
100
30
10
3
(a)
(b)
0
5
10
15
20
25
30
$\frac{x}{a}$
E_e^p

Figure 8 Electric Field in vicinity of Conductive Elliptical Cylinder

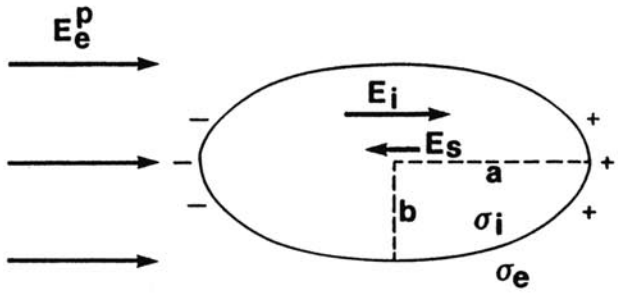

Figure 9 Electric Field in vicinity of Conductive Prolate Spheroid

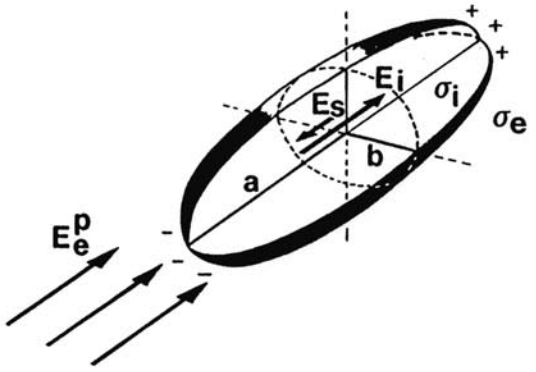

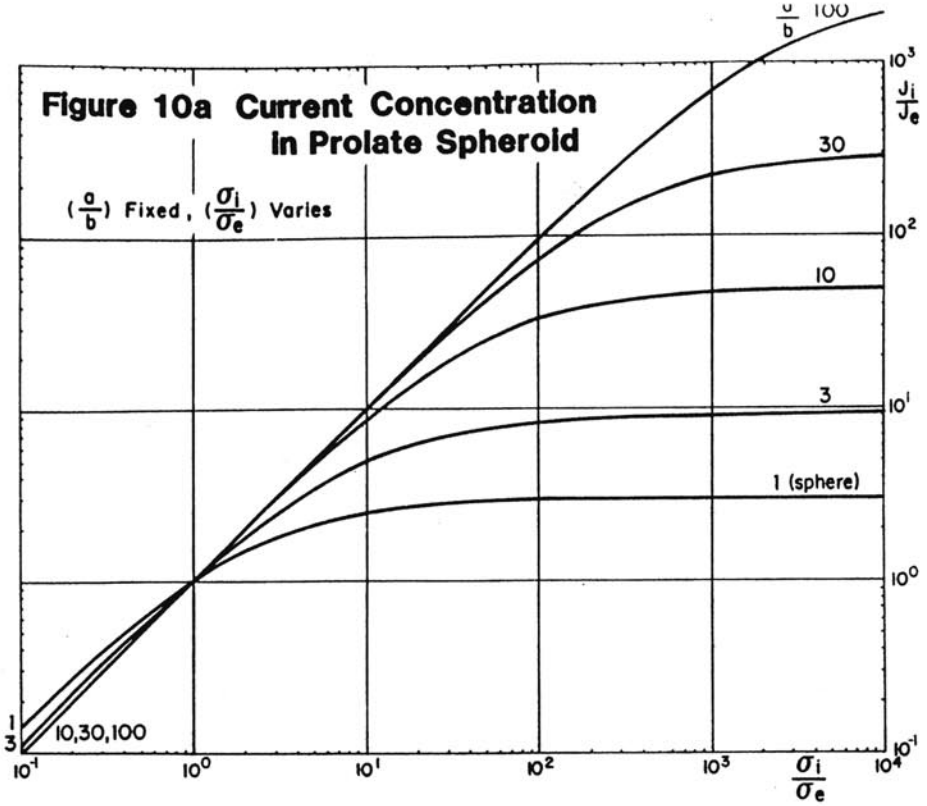
Figure 10a Current Concentration in Prolate Spheroid
(a/b) Fixed, (σi/σe) Varies
a/b 100
30
10
3
1 (sphere)
1/3 10,30,100
Ji/Je
σi/σe

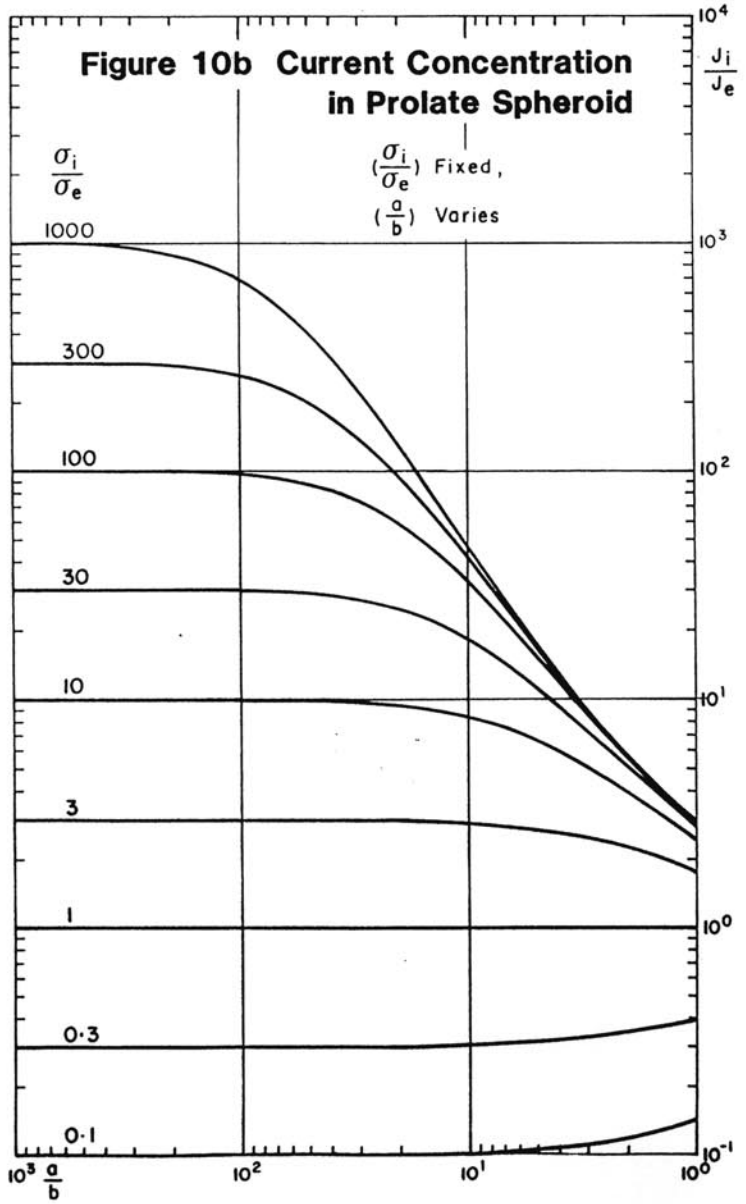
Figure 10b Current Concentration in Prolate Spheroid
(σi/σe) Fixed,
(a/b) Varies
σi/σe
1000
300
100
30
10
3
1
0·3
0·1
Ji/Je
a/b

Figure 11 Current Flow In and Near Spheroid

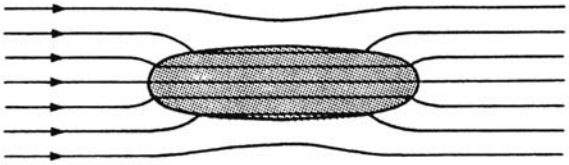

(a) Conductive Spheroid

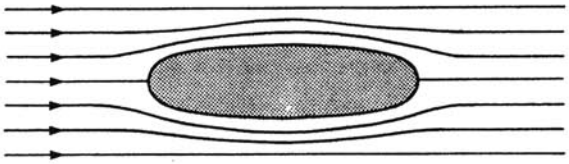

(b) Infinitely Resistive Spheroid

Figure 12 Magnetic Field in vicinity of Conductive Prolate Spheroid

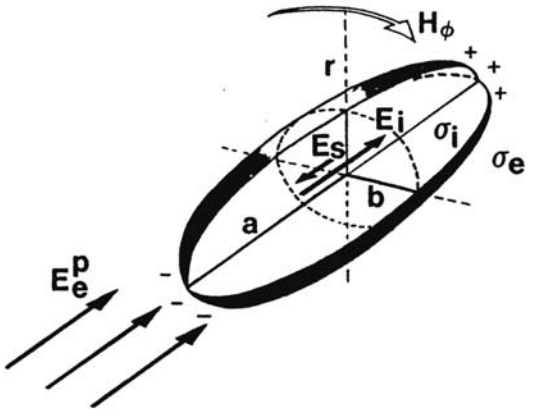

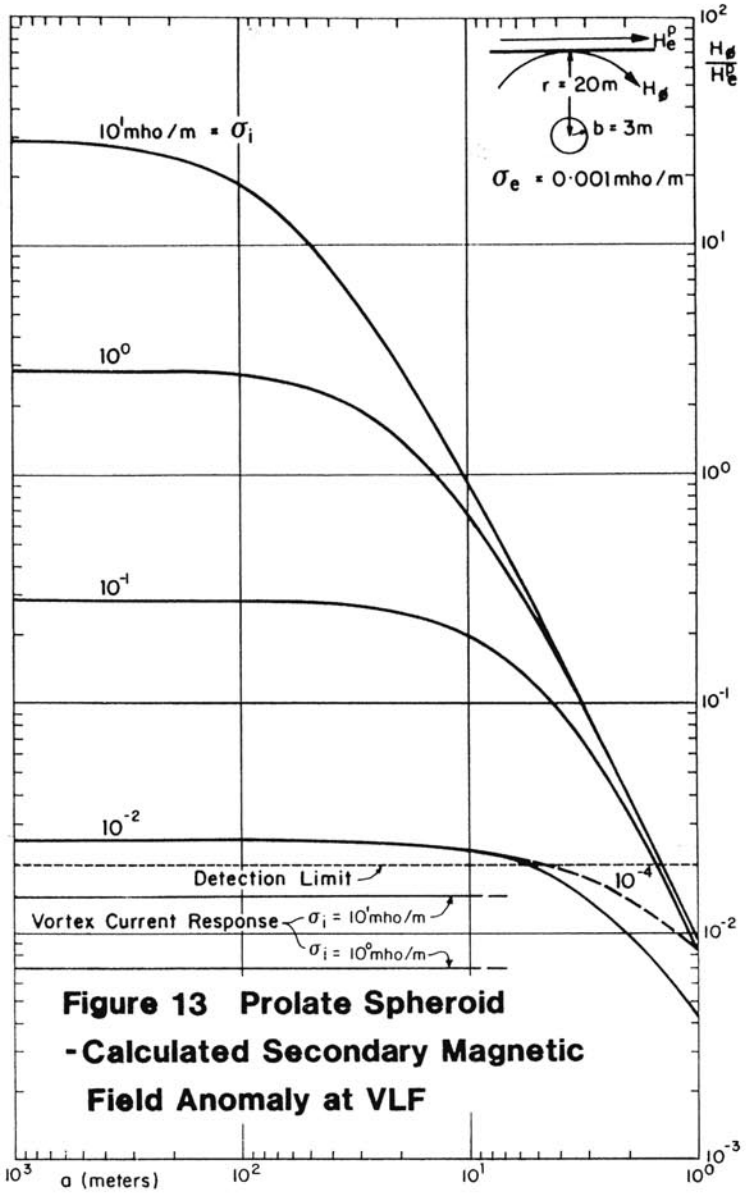

Figure 13 Prolate Spheroid - Calculated Secondary Magnetic Field Anomaly at VLF

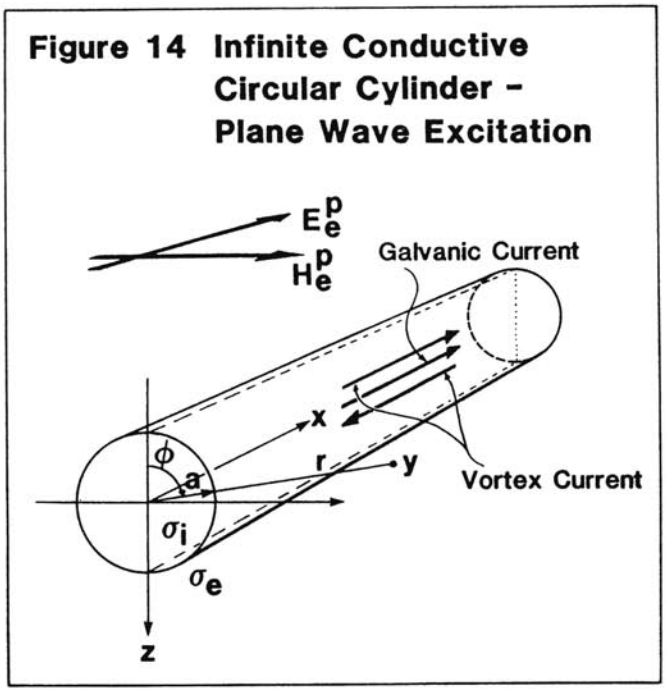

Figure 14 Infinite Conductive Circular Cylinder - Plane Wave Excitation